16th International Conference on
Numerical Simulation of Optoelectronic Devices

NUSOD

SYDNEY 2016

PROGRAM HANDBOOK

INVITED TALKS

POSTER SESSIONS

TUTORIALS

Sydney Nanoscience Hub
The University of Sydney
Camperdown, Sydney, Australia
11 - 15 July 2016

WWW.NUSOD.ORG/2016

The NUSOD Committee gratefully acknowledges the following contributers for their support of the 16th International Conference on Numerical Simulation of Optoelectronic Devices.

cudos
An ARC Centre of Excellence

IEEE

IEEE photonics Society
Transforming science into technology™

THE UNIVERSITY OF SYDNEY

UNIVERSITY OF TECHNOLOGY SYDNEY

MACQUARIE University

COMSOL MULTIPHYSICS®

SYNOPSYS®
Silicon to Software™

CONTENT

PROGRAM-AT-A-GLANCE

MONDAY · 11 JULY

08:30-09:45	Registration
09:45-10:00	Welcome Address
10:00-11:50	Highlights from Down Under (Steel)
11:50-13:00	Lunch (individual)
13:00-14:50	Laser Diodes I (Ryu)
14:50-15:20	Afternoon Tea
15:20-17:00	Novel Materials (Auf der Maur)
17:00-19:00	Poster Session I & Reception (Poulton)

TUESDAY · 12 JULY

08:00-08:30	Registration
08:30-10:00	Novel Devices (Willatzen)
10:00-10:30	Morning Tea
10:30-12:30	Light-Emitting Diodes (Eichler)
12:30-13:40	Lunch (individual)
13:40-14:40	Plasmonics (Kuhlmey)
14:40-15:10	Afternoon Tea
15:10-16:30	Photodetectors (Martyniuk)
16:30-18:30	Poster Session II (de Sterke)

WEDNESDAY · 13 JULY

08:00-08:30	Registration
08:30-10:00	Solar Cells (Wu)
10:00-10:30	Morning Tea
10:30-12:20	Photonics (Bardella)
12:20-12:50	Lunch (served in Harry Messel Foyer)
13:00	Bus departure from Main Quadrangle
14:00-16:30	Taronga Zoo Excursion
17:00-18:30	Harbour walk and/or pre-dinner refreshments
18:30-22:00	Conference Dinner, incl. Awards of Poster Prizes and Prokhorov Centennial Presentation

THURSDAY · 14 JULY

08:00-08:30	Registration
08:30-09:40	Numerical Methods (Koprucki)
09:40-10:10	Morning Tea
10:10-12:00	Laser Diodes II (Dumitrescu)
12:00-13:30	Lunch (individual)
13:30-15:20	Nanostructures (Marquardt)
15:20-15:45	Afternoon Tea
15:45-16:30	Postdeadline Session (Piprek)
16:30-16:40	Closing Remarks

FRIDAY · 15 JULY

08:30-12:00	Crosslight Tutorial on Optoelectronics
08:30-12:00	COMSOL Tutorial on Optomechanics
13:00-16:30	Synopsys RSoft Tutorial on Mixed-Level Optics

VENUES

NUSOD 2016 will be held in the **Sydney Nanoscience Hub** (A31), behind the School of Physics Building (A28), Camperdown Campus, University of Sydney.

I'M LOOKING FOR ...

NUSOD VENUES

Sydney Nanoscience Hub	H6
The Quadrangle	J3

FOOD AND DRINKS

The Quadrangle, University Place	J3
New Law Building	K5
Holme Building	G2
Wentworth Building	L7
Carslaw Building	L6
Manning House	H4

MUSEUMS AND GALLERIES

Macleay Museum	H2
Nicholson Museum	J3
University Art Gallery	J2
Graffiti Tunnel	G3

LIBRARIES

Badham	G3
Fisher	K3
Herbert Smith Freehills Law Library	K4
Medical (Bosch 1B)	E7
SciTech (Jane Foss Russell)	L7

OTHER

First aid, Eastern Avenue	K4
New Law Building carpark	K5
Shepherd Street carpark	O6
Redfern station	O9
Newtown	A-G11

CAMPERDOWN AND DARLINGTON CAMPUS MAP

VENUES

Registration desk and **food & beverage stations** are located in the Harry Messel Foyer on **Level 3**.

The **Conference Sessions** from Monday to Thursday are held in the **Harry Messel Lecture Theatre** (access to the Harry Messel Lecture Theatre on Level 3 and Level 4).

LEVEL 3

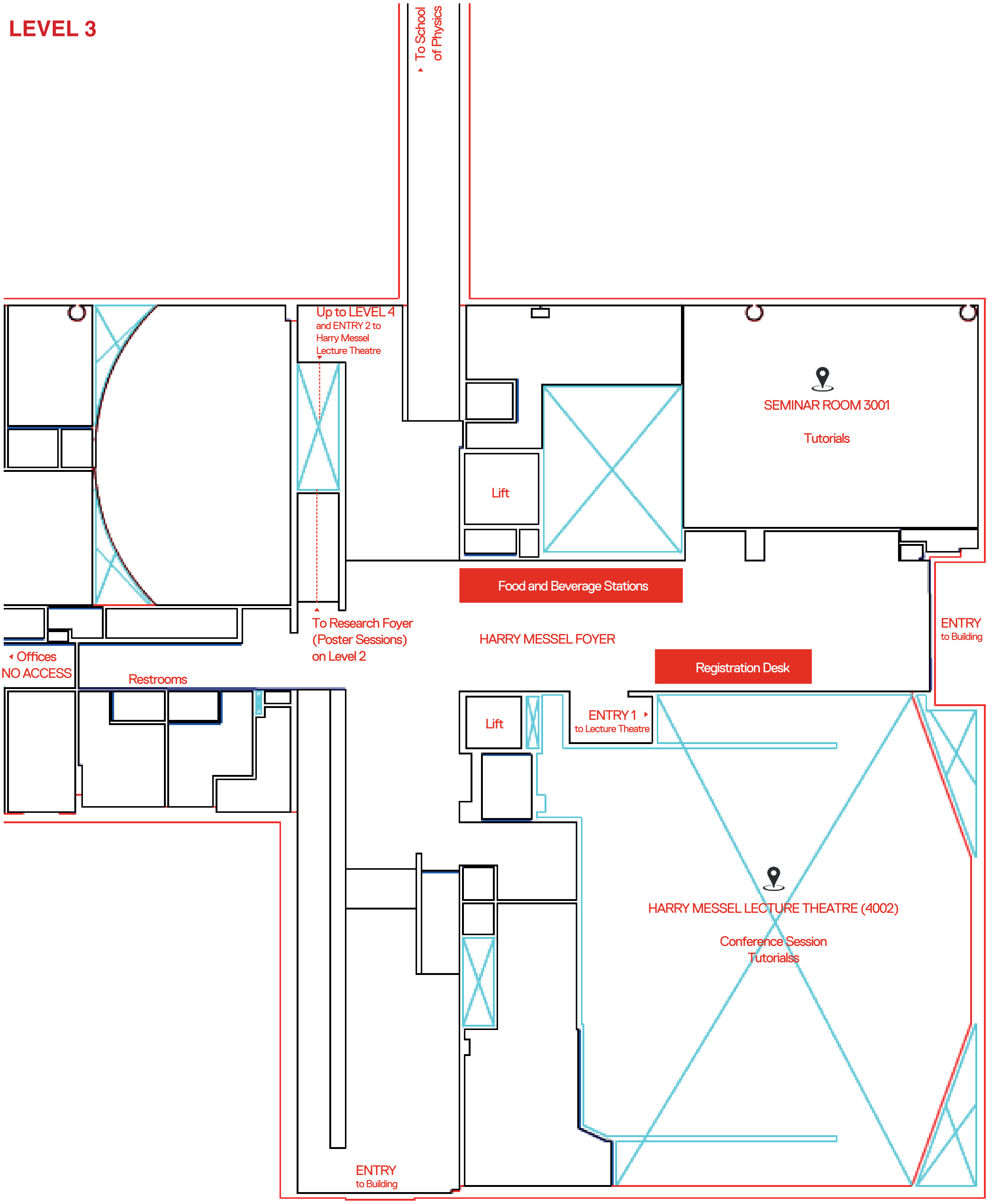

The **Tutorials** on Friday are held in the Harry Messel Lecture Theatre 4002, Seminar Room 3001 and Seminar Room 4003 on **Level 3** and **Level 4.**

LEVEL 4

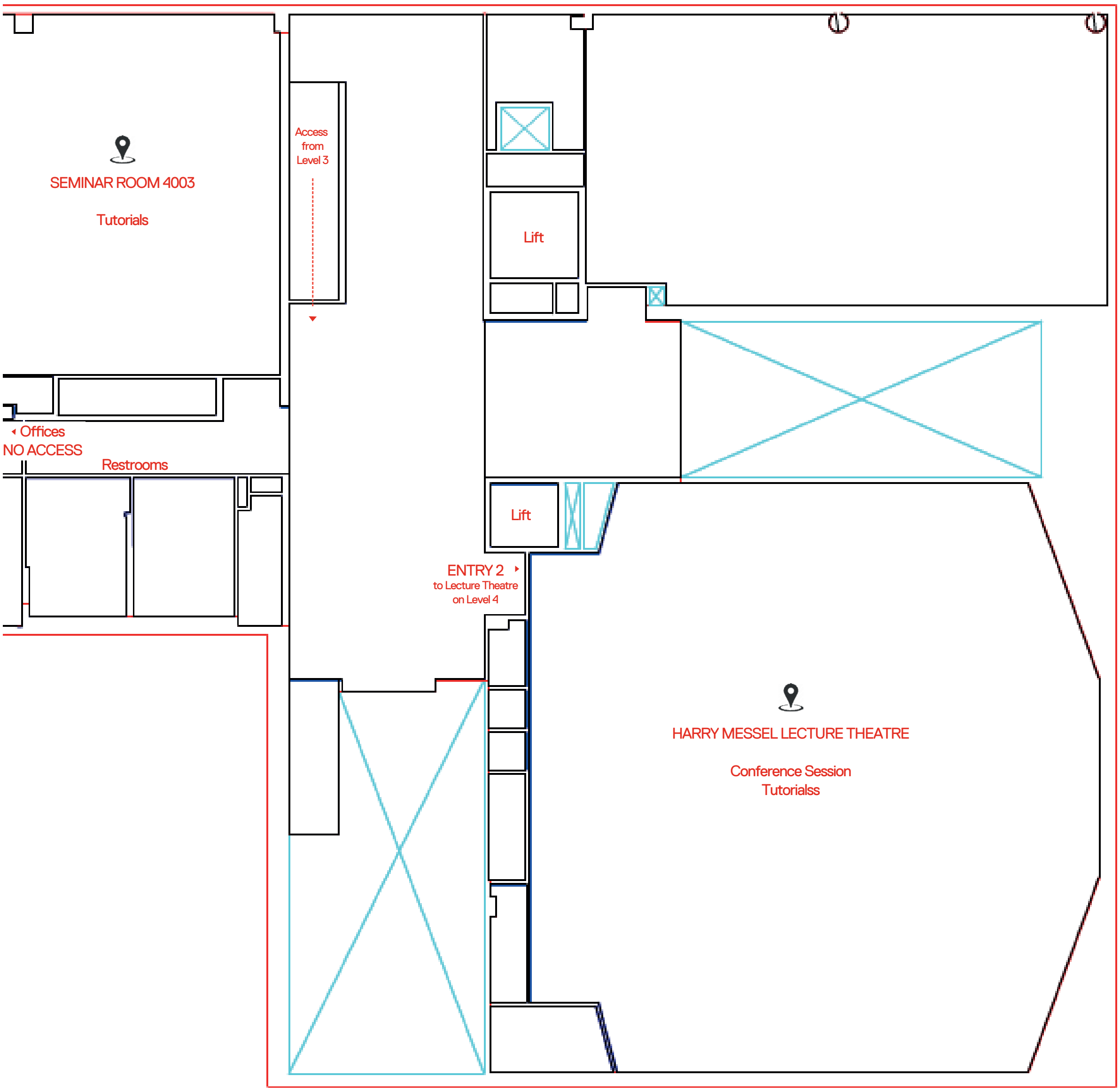

The **Poster Sessions** and **Welcome Reception** on Monday and Tuesday are held in the Research Foyer on Ground Floor **Level 2**. To access the Research Foyer, please follow the 'NUSOD Poster Sessions' signage.

LEVEL 2

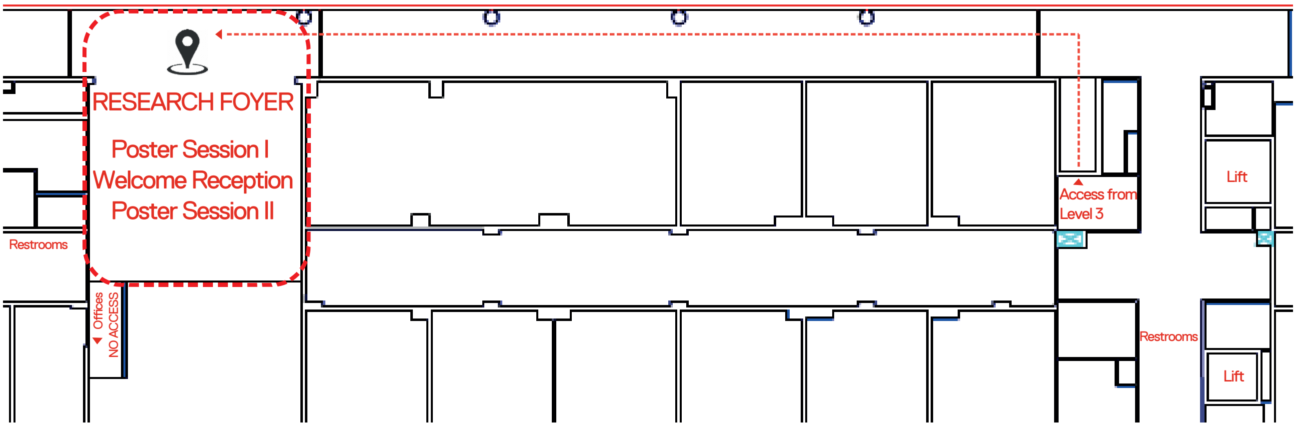

GENERAL INFORMATION

REGISTRATION

On-site Registration and Badge Pick-up Hours

Monday	08:30 to 09:45
Tuesday	08:00 to 08:30
Wednesday	08:00 to 08:30
Thursday	08:00 to 08:30

Pre-registered participants or on-site registrants may pick up their conference materials at the registration desk. All delegates will receive a name badge upon arrival. The name badge serves as your entrance ticket to the sessions, please make sure that you wear it at all times during all conference activities. Inside your lanyard you will find the conference dinner ticket, excursion ticket and your ferry ticket from Tarango Zoo to Circular Quay. Please bring the ferry ticket with you to the excursion.

NUSOD Cashier

Registration Area ▪ Open during registration hours

If you are paying by cash as part of your on-site registration, or have questions regarding your registration, please contact Ms Silke Weiss on +61 2 9351 2637 or email silke.weiss@sydney.edu.au.

INTERNET ACCESS

Complimentary WiFi Internet access is available. Make sure your wireless adapter is set to dynamically obtain an IP address. To access the network connect to 'UniSydney-Guest'.

Enter credentials:

- Username: nusod2016
- Password: 78421747

NUSOD CONFERENCE APP

NUSOD 2016 has gone mobile! Search and browse the program, special events, participants, and more, with the free conference app available for iPhone and Android Phone. Get your app here: http://guidebook.com/g/nusod

Android and iOS users:

1. Tap the 'Download' button to download the free Guidebook app
2. Open Guidebook and you can find your 'NUSOD 2016' guide

The app is also available through any web/mobile browser:
http://guidebook.com/guide/66070

INSTRUCTIONS FOR ORAL PRESENTATIONS

Please check the program well in advance for the date and time of your presentation. Presenters are asked to:

- Please arrive at the Harry Messel Lecture Theatre 10 minutes before the start of the session.
- Please upload your PowerPoint file onto the device in the room for presentation and make sure that your file runs appropriately.

If you wish, you may use your laptop that has a VGA output for the presentation.

POSTER SETUP INSTRUCTIONS

The poster sessions will be held in the Sydney Nanoscience Research Foyer (see map on page 7).
All registered attendees are invited to attend the poster sessions. This event will provide an opportunity to meet with colleagues, network, and view the poster papers. Authors will be present at their posters to answer questions and provide in-depth discussions regarding their work.

Setup Monday, 11 July	15:15 to 16:30
Poster Session I & Weclome Reception: Monday, 11 July	17:00 to 19:00
Setup Tuesday, 12 July	10:00 to 16:00
Poster Session II: Tuesday 12 July	16:30 to 18:30

POSTER AUTHORS: Poster boards will be available on Monday afternoon at 15:15. Please set up your poster during the afternoon tea break, and plan to stand by your poster during the poster sessions. Poster must be removed from the boards following the poster session. Poster that remain on the boards will be discarded.

SOCIAL EVENTS

Welcome Reception.......... Monday, 11 July, 17:00 to 19:00 in the Research Foyer
Excursion.......... Wednesday, 13 July, 13:00 to 18:30 at Taronga Zoo and Sydney Harbour
Conference Dinner.......... Wednesday, 13 July, 18:30 to 22:00 at Italian Village at The Rocks

NOTICES AND MESSAGES

Notices and messages related to conference activities and any changes to the conference program will be displayed at the Registration Desk and on the mobile app.

URGENT MESSAGE LINE

An urgent message line is available; please call Associate Professor Christopher Poulton on +61 2 9514 4370 or Professor Martijn de Sterke on +61 2 9351 2906.

TRANSPORT

How to get to the University of Sydney

The Sydney Nanoscience Hub is located at the Camperdown Campus of the University of Sydney - close to main public transport routes on the train and bus lines (see map on page 5).

By train

Redfern is the closest train station. It is a 10-minute walk to the main campus, and a fairly steady flow of students walks the route via Lawson Street and Abercrombie Street at all times of day and evening. Central station is a 15-minute walk along City Road and George Street; however, buses to and from Central are frequent and easy to catch from Parramatta Road or City Road.

By bus

If you are arriving by bus, there are convenient stops on Parramatta Road and City Road at our main entrances. Use the campus map to locate the closest bus stop to your destination.
For stops on City Road (closest to Darlington Campus) catch routes 422, 423, 426, 238 or metrobus M30 from George Street or Railway Square.

By taxi

When looking for a cab, use the ranks or call:

- Taxi Combined Services 13 33 00
- GM Cabs 131 001
- Legion Cabs 13 14 51

Parking

Some of our campuses offer casual and permit parking. With limited parking on campus, we encourage you to use public transport, walk or cycle in.

Useful Public Transport weblinks

- Public Transport Planner: http://www.cityofsydney.nsw.gov.au/explore/getting-around/public-transport
- Taxi info: http://www.cityofsydney.nsw.gov.au/explore/getting-around/public-transport/taxis

GENERAL INFORMATION

FOOD AND BEVERAGE SERVICES

Refreshment breaks

Monday .... 08:30 to 09:45 and 14:50 to 15:20
Tuesday .... 08:00 to 08:30 and 10:00 to 10:30 and 14:40 to 15:10
Wednesday .... 08:00 to 08:30 and 10:00 to 10:30
Thursday .... 08:00 to 08:30 and 09:40 to 10:10 and 15:20 to 15:45

Complimentary barista coffee / tea and pastries will be served twice daily (except Wednesday afternoon) and during registration hours in the Harry Messel Foyer.

Daily Lunches

Lunch is not included in conference registration (except on Wednesday); the scheduled lunch break time is open for attendees to explore some of the local restaurants and area.
Sydney Uni Campuses have more than 30 places to eat, ranging from healthy juice bars to hearty pub meals (see map page 5). There are also a few hundred cafes and restaurants within a few blocks of campus in Newtown on King Street (please see walking route to Newtown on map - page 5). Download the Sydney Uni app for on-the-go access to campus maps that will guide you to the closest eateries: sydney.edu.au/mobile

EATERIES ON CAMPERDOWN CAMPUS

Bosch Catering Outlet, Bosch Lecture Theatre, Western Avenue Choose from a great range of home-made Turkish sandwiches. Also available are chips, hamburgers and coffee. An inside seating area is provided.	Carslaw Coffee Cart, Carslaw Building A convenient one-stop-shop for snacks, confectionery, and hot and cold beverages.	Courtyard Restaurant and Bar, Ground Floor, Holme Building Mediterranean-inspired menu offers a range of pizza, pasta and salads, with gluten-free and vegetarian options. Australian wine and craft beers on tap.
Fisher Coffee Cart, outside Fisher Library Open seven days during semester for coffee, snacks and cold drinks.	Footbridge Station, Ground Floor, Holme Building Sandwiches, salads, pies and sausage rolls as well as cakes to go with barista-made coffee.	The Grandstand, No. 1 Oval, University of Sydney Blackburn Circuit Sports bar, bistro and function centre.
Lettucehead, Ground Floor, Manning House Serves a variety of salads, sandwiches, fruit salad, yogurt, wraps, baguettes, soups and beverages.	Manning Bar, Level 2, Manning House Offers entertainment as well as alcoholic beverages and pub style meals. Seating can be found inside and outside on the balcony	Manning Grill, Level 2, Manning House On the balcony next to Manning Bar. Offers pub-style meals with daily specials.
Manning Kiosk, Manning Road Located on Manning Road is Manning Kiosk with ready-made sandwiches, wraps, hot pastries, cakes, and hot and cold beverages.	Miso Honi, Ground Floor, Manning House Modern Asian including laksa, sushi, noodles, fried and steamed rice dishes, steamed dumplings, pad thai, teriyaki chicken, rice paper rolls and gyozas.	Ralph's Café, Arena Sports Centre One of our renowned culinary icons, Ralph's Café has been serving up home-style food and coffee to sleep-deprived students for more than 30 years. A popular choice is the Nutella cream croissants for an afternoon sugar hit.
Taste Baguette, Law School Annex Boutique roasted coffee, fresh baguettes made to order and a dangerously tempting selection of sweets. Conveniently located along Eastern Avenue, you can pick up lunch or coffee on your way to class.	Caffe Tra Baci, Ground Floor, Manning House Enjoy a barista-prepared Vittoria 100 percent Arabica coffee, a sweet treat, lunch or snack. Open daily from 8am all year round.	Xquisito, Ground Floor, Manning Courtyard Hot jacket potatoes, savoury and sweet crepes, smoothies, fresh juices and frappes.

Zabeli, Level 1, Manning House Bacon and eggs, toasted sandwiches, burgers, lasagne, pizza, hot chips and wedges, wraps, focaccias, risotto, cakes and coffee.

EATERIES ON DARLINGTON CAMPUS

Belle Vie Cafe, Level 1, Wentworth Building Beautiful desserts, cakes and meals including burritos, turkish bread with chicken schnitzel or cheese and roast veggies, light and healthy wraps, fresh pork rolls with delicious filling and more.	Laneway, Level 3, Wentworth Building Freshly baked waffles, artisan breads, freshly ground sustainable coffee, cakes and gourmet sandwiches. The only place on campus with all day breakfast.	Hermann's Bar, Wentworth Building A relaxed atmosphere in which to study or compute (wireless internet available) while enjoying a fine selection of beers, wine, hot beverages and food.
Jewel of India, Level 2, Wentworth Building Selection of hot Indian dishes, meats from the tandoor, roti rolls and sweets.	Little Asia, Level 2, Wentworth Building Modern Asian cuisine. Noodles, fried rice, steamed and wok fried dishes.	Raw, Level 2, Wentworth Building Healthy salads, rolls, juices and smoothies.
Snack Express, Level 2, Wentworth Building This outlet offers gourmet sandwiches, a range of pastries, pies and great coffee. Open at 7.30am for breakfast through to late all year.	Uni Brothers Kebabs, Level 2, Wentworth Building Kebabs, salads, hot chips, burgers, pide and pizza.	Cafe Azzuri, Plaza – Jane Foss Russell Building Savoury and sweet crepes.
Easyway Tea, Plaza – Jane Foss Russell Building Variety of beverages.	Parma Cucina and Bar, Shop 3, Plaza, Jane Foss Russell Building Sandwiches, coffee, hot meals, outdoor seating. Licensed.	Subway, Plaza, Jane Foss Russell Building Choose-your-own-filling sandwiches.
The Forum Restaurant, Darlington Centre, 174 City Road This two-storey heritage residence houses a full-service indoor/outdoor restaurant and bar.	Boardwalk Cafe and Diner, next to Co-op Bookstore Coffee, Asian cuisine, pizza, sandwiches.	University Sports and Aquatic Centre Cafe Coffee, sandwiches and light meals. Open seven days.
Engineering Café, PNR Building, Maze Crescent Options include coffee, fresh salads, the weekly meal deal, hamburgers and more. Indoor and outdoor seating is available.	The Hearth Café, Wilkinson Building, City Road Hot and cold beverages, sandwiches, wraps, cakes and pastries.	Daylight Savings Bar, Courtyard, Seymour Centre Opens every Thursday, Friday and Saturday from 5pm until late.
The Downstairs Bar, Sound Lounge, Seymour Centre An intimate bar with table seating and serves light pre-show snacks. It is also the perfect bar for post show drinks as three nights a week it is transformed into the Sound Lounge with live music Thursday to Saturday.	The Everest Bar, Seymour Centre With expansive floors and walls the Everest Bar hosts regular exhibitions of sculpture and painting curated by Defiance Gallery in Newtown. It is the perfect bar for pre- and post-show functions and is a favourite for opening and closing night parties.	The Coffee Cart, Main Foyer, Seymour Centre Open before shows, serving great coffee, light snacks and alcoholic beverages.

EXCURSION AND DINNER INFO

WEDNESDAY, 13 JULY 2016, 12:30 - 22:00H

Visit Australia's unique wildlife against the spectacular backdrop of Sydney Harbour!

- Lunch will be provided in the Harry Messel Foyer from 12:20pm
- Taronga Zoo Website: taronga.org.au/taronga-zoo
- Please take your ferry ticket with you - you can find it inside your neck wallet

12:20	Lunch will be provided in the Harry Messel Foyer
12:50	Meet in Harry Messel Foyer to walk over to bus departure point 'Quadrangle'
13:00	Departure to Taronga Zoo Bus departs from the 'Quadrangle' at 1pm, see map below
14:00	Taronga Zoo Guided Walk From one end of the Zoo to the other, an experienced guide will take you through the best displays, the most exciting animals, and introduce you to Australia's native wildlife. You will be able to learn about Australia's native animals from expert guides and get some close opportunities with Macropods. Included is also a round trip on the Sky Safari cable car - discover why Taronga is known as "The Zoo with a View".
16:42 / 17:12	Return to Sydney Harbour by ferry from Taronga Zoo Wharf to Circular Quay: • Ferry ticket is inside your neck wallet • Ferry F2 departs every 30min from 16:42 onwards • Timetable: transportnsw.info/resources/documents/timetables/F2-taronga-zoo.pdf
17:00 - 18:30	Harbour walk and/or pre-dinner refreshments We will break into several groups to either walk in the environs of Circular Quay and the Opera House, or visit one of the local pubs on the route to the dinner venue. Local organisers will lead these groups. Note that drinks at each site are self-purchased. • Group 1: Walk around the Opera House and briefly into the lower part of the Botanic Gardens to view the Harbour at Dusk. Time permitting we will stop at the Opera Bar on the Opera House Concourse (ends with 15 minute harbourside walk to dinner venue) • Group 2: Drinks at the Opera Bar facing the Harbour Bridge as night falls (ends with 15 minute harbourside walk to dinner venue) • Group 3: Orient Hotel in The Rocks (Bar and lounge; shortest walk) • Group 4: Observer Hotel in The Rocks (Traditional Australian style hotel bar with craft beers; equal shortest walk)
18:30 - 19:00	Pre-dinner drinks at the Italian Village
19:00 - 22:00	Dinner at the Italian Village, incl. award of poster prizes and Prokhorov Centennial Presentation

In case you miss the excursion, you may go by taxi to the dinner restaurant Italian Village, address: Italian Village, 7 Circular Quay West, The Rocks NSW 2000

Walking route to bus departure point

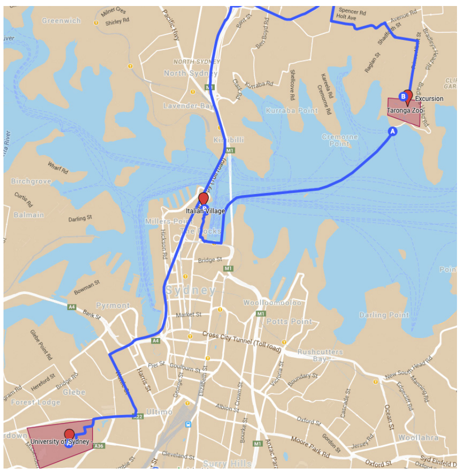

Excursion round trip

The **Conference Dinner** is held in the Florence Room (second floor) at the **Italian Village**.

- Address: Italian Village, 7 Circular Quay West, The Rocks NSW 2000
- Access via Circular Quay West or Hickson Road Door #27 - please look for the NUSOD Conference Dinner signage

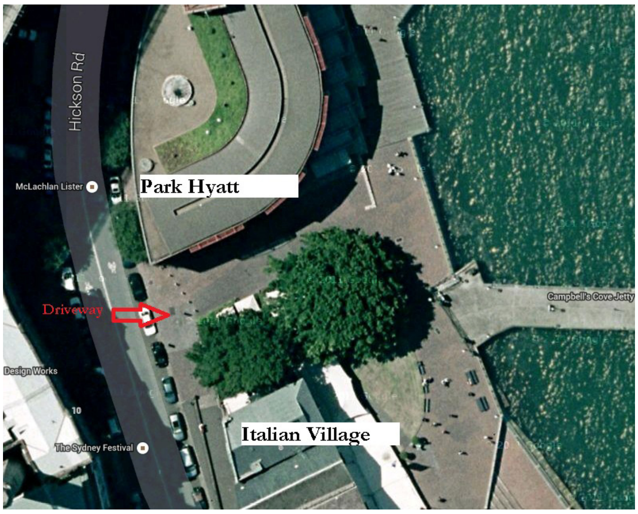

Bird's-eye view of Italian Village

View of entry via Hickson Road

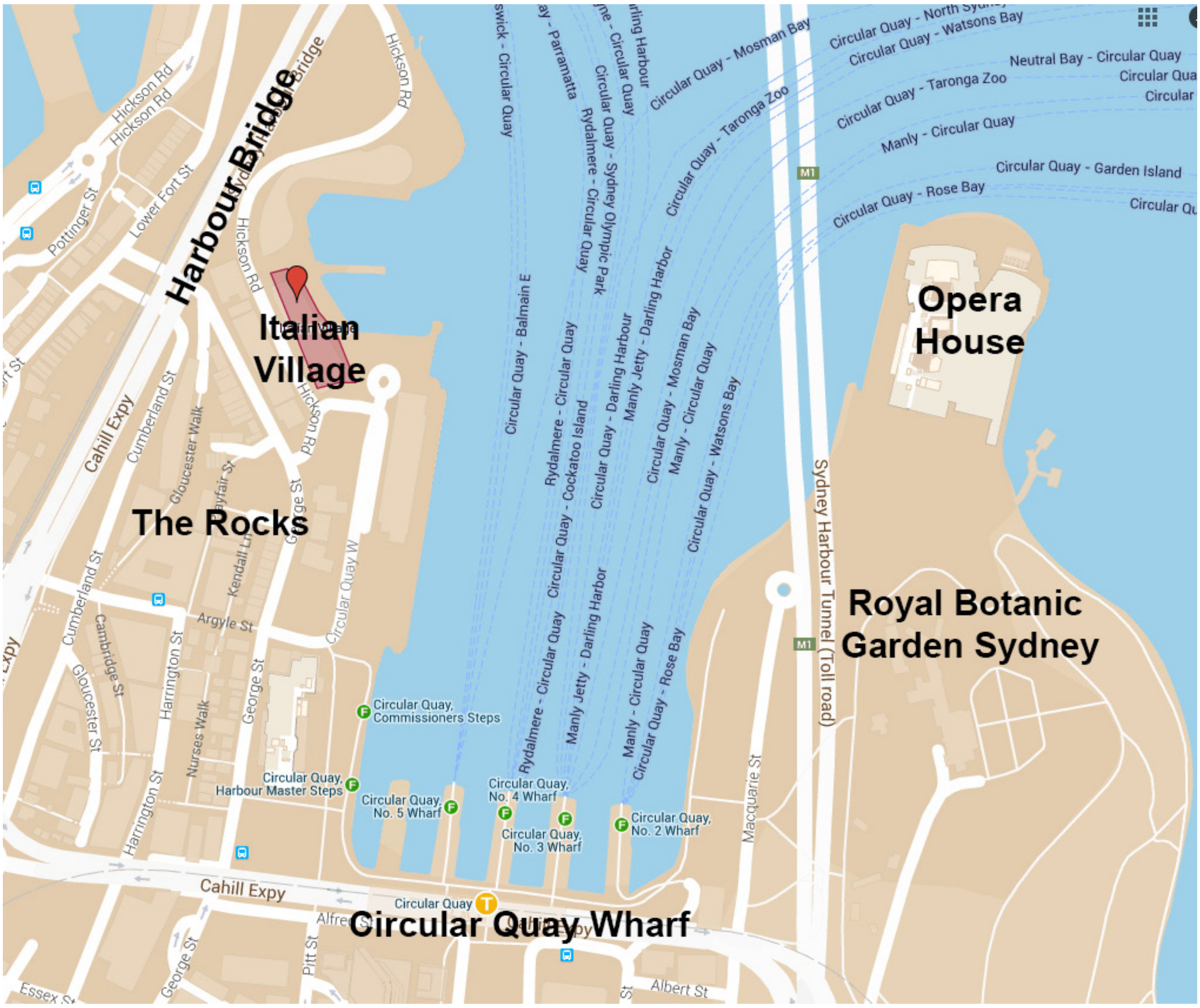

Sydney Harbour Map

NUSOD

SYDNEY 2016

16th International Conference on Numerical Simulation of Optoelectronic Devices

July 11th-15th 2016

Postdeadline programme

15:45-16:30, Thursday July 14th, 2016

Session	**Title**	**Authors/Affiliation**
ThPD1 15:45	Modeling and Analysis of GaAs Solar Cells for Conversion Efficiency Improvement by Reducing Reflection Losses	Devanandh Chandrasekar [1] and Narottam Das[1,2] [1] *University of Southern Queensland, Australia;* [2]*Curtin University, Australia*
ThPD2 16:00	Design of Plasmonic Modulator Based on Vanadium Dioxide	Miao Sun, Stuart Earl, William Shieh and Ranjith Rajasekharan Unnithan; *University of Melbourne, Australia*
ThPD3 16:15	Exact numerical modelling for finite samples of discrete metamaterials	Mikhail Lapine *University of Technology Sydney, Australia*

Modeling and Analysis of GaAs Solar Cells for Conversion Efficiency Improvement by Reducing Reflection Losses

Devanandh Chandrasekar[1] and Narottam Das[1,2] *Senior Member, IEEE*
[1]School of Mechanical and Electrical Engineering, University of Southern Queensland, QLD 4350, Australia
[2]Department of Electrical and Computer Engineering, Curtin University, Perth, WA 6845, Australia
E-mail: cdevanandh@gmail.com and narottam.das@usq.edu.au

***Abstract*— Finite difference time-domain (FDTD) method is used to design, simulate and calculate the light trapping properties of nano-gratings over the GaAs substrate. The simulation results show that the light reflection loss reduces ~27% using the nano-grating structure when compared with a conventional or flat type solar cells.**

***Index terms*— Conversion efficiency, FDTD simulation, GaAs substrate, Light reflection, Nano-grating structure, Solar Cells.**

I. INTRODUCTION

As an alternative of fossil fuel energy, solar cells can provide an efficient and environmental friendly solution for green earth. Solar cells were discovered in the 19th century, which has attracted to different scientists around the world to conduct research in this area to improve the conversion efficiency and also in an aim to attain minimized CO_2 reduction. In general, solar panel emits 16~21g/kWh of CO_2 for roof and ground-mounted CdTe PV panels with solar irradiance of 1700kWh/m2 /yr in Southern Europe [1]. My Queensland Government survey reported that electricity generation is the largest source of CO_2 emission [2]. Reduction of CO_2 emissions can be achieved gradually by utilizing the renewable energy sources, such as solar or PV and wind power systems. The conversion efficiency of solar cells are affected by different types of losses. However, the light reflection loss has significant impact to reduce the conversion efficiency of solar cells. They have a very significant appeal over light absorption property of a solar cell. In-order to overcome this issue, thin film anti-reflective (AR) coating is used to minimize the reflection losses but the AR coating can work for certain wavelengths only. However, there are some drawbacks on using the AR coating, such as it might have thermal and adhesive mismatch with the substrates. Hence, subwavelength grating (SWG) structures have been identified as promising candidate for realising high conversion efficiency in solar cells due to their low reflection losses. If the pitch (or period) of a single grating structure is less than the wavelength of the incident light, it behaves like a homogeneous medium with an effective refractive index [3]. Therefore, the SWG structures provide gradual changes in refractive index that ensure an excellent antireflective and light trapping properties compared to a planar or flat type thin film [3-4]. Finite-difference time domain (FDTD) simulation tool is used to design, simulate and analyze the data associated with properties of light transmission, reflection and absorption in the nano-grating structure [5]. For simulations, we have considered triangular, trapezoidal, and rectangular nano-grating shapes. All the nano-grating shapes height is varied during the simulation process in-order to find the best possible result that can capture more incident lights into the GaAs substrate for high conversion efficiency of the solar cells [6].

II. DESIGN OF NANO-GRATING STRUCTURE

In this section, we discuss the nano-gratings shape design and modeling of nano-structured gratings (i.e., SWG structures). The nano-grating shapes are: (i) rectangular, (ii) trapezoidal with different aspect ratios (i.e., 0.1 ~ 0.9), and (iii) triangular. Here, we discussed only the triangular shaped nano-gratings as shown in Fig. 1. For triangular-shaped nano-gratings, the aspect ratio is '0' (i.e., the top length of the trapezoid is zero compared to the base length of the trapezoid). This shape is used for the simulation and analyzed the results for light reflection, transmission and absorption for the SWG structures.

In Fig. 1, there are two lines above the nano-grating structures, such as red and green lines, they represent the incident and reflected lights, respectively. However, in the substrate there are two lines which represent the transmission line 1 and 2. The triangular shaped nano-structured gratings are designed on top of the GaAs substrate.

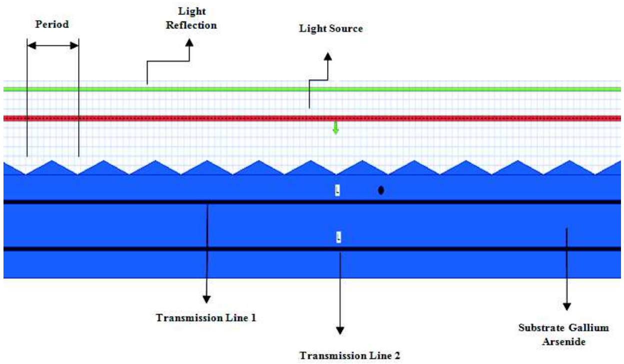

Fig. 1. Schematic diagram of a triangular shaped nano-gratings on top of the semiconductor (GaAs) substrates.

The material Gallium Arsenide (GaAs) is used for the substrate and the nano-grating structure. The incident light directly hits on top of the nano-structure. A major portion of light is absorbed by the nano-grating zone due to the gradual change of refractive

Post-Deadline Paper ThPD1

index in the nano-grating zone, some portion of the light is reflected and the remaining portion of the light is transmitted through the GaAs substrate. Since the light absorption rate of this nano-grating is high, it provides a steady change in the refractive index and ensuring a phenomenal AR medium alongside a light trapping capacity in comparison to other films. The refractive index change can be calculated using following equation,

$$\frac{n_1}{n_2} = Sin\left(\frac{\theta_2}{\theta_1}\right) = \frac{\lambda_2}{\lambda_1} \quad (1)$$

where, n_1 and n_2 represents the medium of refractive index. θ_1 and θ_2 represents the angle of incidence and angle of refraction. λ_1 and λ_2 represents the wavelength of incident medium V_1 and refracted medium V_2, respectively. Fig. 2 shows the relationship between the angle of incidence and angle of refraction using Snell's law.

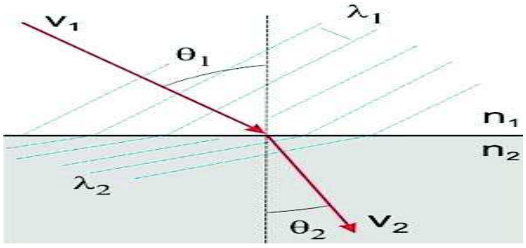

Fig. 2. Relationship between the incidence angle and refraction angle.

III. Simulation Results and Discussion

Fig. 3 shows the light reflection losses spectra for several nano-grating heights (i.e, 100 nm ~ 400 nm) with the period of 830 nm. For this simulation, the incident light wavelength is kept constant at 830 nm. The simulated results show that when the nano-gratings height increases then the light reflection reduces and reaches to the saturation of light reflection at 300 ~ 350 nm. These results show that the nano-grating height is ~300 nm gives minimum light reflection. It has also confirmed that the light refelection for 300 nm and 350 nm grating height is very close. This nano-grating height for light reflection is minimum and it reaches to the saturation, which has the similar tendency as reported [5]. When the nano-grating height decreases further, such as 100 nm, the ligth reflection increases.

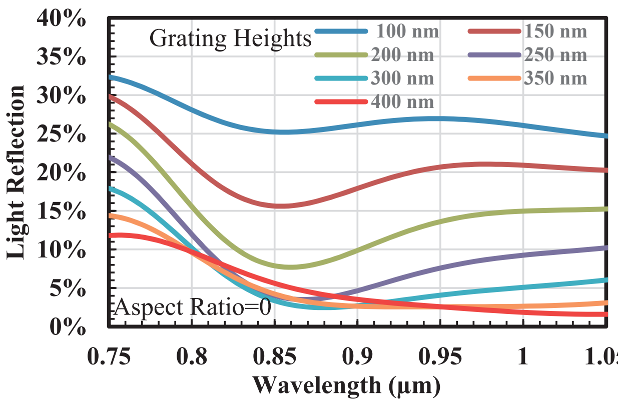

Fig. 3. Light reflection spectra for triangular shaped nano-grating structure with the grating pitch 830 nm.

Fig. 4 shows the light absorption spectra for different nano-grating heights, such as 100 nm to 400 nm. The simulated results show that with the increase of nano-grating heights the light absorption rate increases and reaches the saturation at 300 ~ 400 nm. It also observed that light absorption rate for 300 and 350 nm is very close, at the wavelength 830 nm. As the nano-grating height decreases, the capacity of light absorption also decreases gradually.

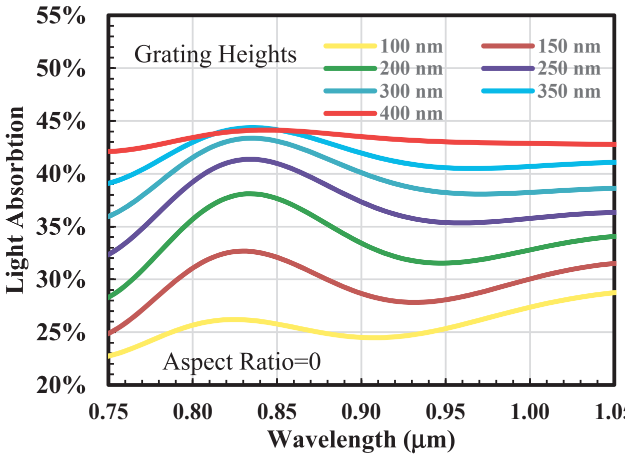

Fig. 4. Light absorption spectra for triangular shaped nano-grating structure with the grating pitch 830 nm.

IV. Conclusion

We have modeled and analyzed the light capturing properties of nano-grating structures with different shapes. For this simulation, FDTD method is used to obtain the results for light transmission, reflection and absorption on GaAs solar cells. It is clear from the simulated results that the triangular shaped nano-gratings absorb more light into the GaAs substrate. This simulation results confirm that the use of nano-grating structure has ~ 27% higher light absorption capacity than the conventional solar cells, hence increase the conversion efficiency of GaAs solar cells. The simulated results are useful for the design and development of high conversion efficiency of GaAs solar cells for a sustainable green earth.

References

1. P. Sinha and J. Laura, "Estimating carbon displacement by solar deployment", *First Solar Sustainable Developement, vol. 2.1, no. 21,* 2012.
2. My Queensland Government Survey Report (May 2015), avaiable in the link https://www.business.qld.gov.au/industry/energy/renewable-energy.
3. Y. M. Song and Y. T. Lee "Simulation of antireflective subwavelength grating structure for optical device applications", *in Proc. of the NUSOD 2009*, Sept. 14~17, 2009, pp. 103-104, Gwangju Institute of Science and Technology, Republic of Korea.
4. J. H. Schmid, P. Cheben, S. Janz, J. Lapointe, E. Post, A. Delage, A. Densmore, B. Lamontagne, P. Waldron, D. -X. Xu, "Subwavelength grating structures in planar waveguide facets for modified reflectivity", *in Proc. of SPIE*, vol. 6796, 67963E1-10, June 2007.
5. N. Das, A. Karar, M. Vasiliev, C. L. Tan, K. Alameh, and Y. T. Lee, "Analysis of nano-grating-assisted light absorption enhancement in MSM-PDs patterned using focused ion-beam lithography", *Opt. Commun., vol. 284, no. 6, pp. 1694-700, 2011.*
6. R. Dewan, M. Marinkovic, and R. Noriega, "Light trapping in thin-film silicon solar cells with submicron surface texture", *Optics express, vol. 17, 2009.*

Design of A Plasmonic Modulator Based on Vanadium Dioxide

Miao Sun, Stuart Earl, William Shieh and Ranjith Rajasekharan Unnithan
Department of Electrical and Electronic Engineering, the University of Melbourne,
Melbourne, Victoria 3010, Australia, miaos1@student.unimelb.edu.au.

Abstract: We present the design of an electrically driven plasmonic modulator that exploits the large refractive index contrast between the metallic and insulating phases of vanadium dioxide to demonstrate high modulation depths in a device with small footprint of 6 um .

I. INTRODUCTION

The modulator is one of the key components required for an optical telecommunication link. A modulator is able to encode a high-speed electronic data stream to an optical carrier wave. Silicon based modulators are widely used in optical communications and can be classified as either resonant or non-resonant[1, 2]. The majority of silicon-based modulators reported so far operate using the plasma dispersion effect in silicon or the Pockels effect in the nonlinear cladding (also known as silicon–organic hybrid (SOH))[2, 3]. Resonant modulators suffer from bandwidth limitations, temperature fluctuations and fabrication tolerances [1, 3, 4]. In contrast, non-resonant modulators operate across a large spectral window and are typically based on a traveling wave configuration. In order to get sufficient modulation depth, there should be long interaction time between the optical and the modulating radio frequency (RF) signal and hence non-resonant modulators are bulky, often up to several millimeters in length. Surface plasmons are surface electromagnetic waves that couple propagating light to charge density oscillations and are confined to the interface between a metal and a dielectric. Plasmonic modulators operating at 40 GHz and 65 GHz have been recently demonstrated in devices with a footprint on the order of 29 μm [1].

Vanadium dioxide (VO_2) is a canonical electro-optic material whose first order insulator to metal transition occurs at temperatures near room temperature (68℃) or adding electric field of $6.5 \times 10^7 V/m$[5]. The phase change of VO2 can happen in picoseconds, which enable the modulator to work at high frequency. Applications of a 3-4 V electric field across an electrode with a nanoscale gap (100 nm) [6] has been reported for photonic switches [7, 8] and optical modulators [5, 8]. The enabling mechanism for many of these devices is utilizing the large refractive index variation of VO2 that accompanies phase change. Here we exploit this element of the phase change to propose a plasmonic modulator to enhance the modulation depth in a small footprint. This approach permits a modulator device footprint of less than 10μm.

II. DEVICE DESIGNS AND RESULTS

Device designs and optimizations were carried out using the finite element method implemented in COMSOL Multiphysics. To demonstrate the optical modulation performance using VO_2, a plasmonic coupling scheme similar to reported in ref [1] was used, which is designed to excite the surface plasmons efficiently by the incident light within C-band wavelength. The refractive indices of VO_2 with respect to wavelength for both semiconductor and metallic phases were experimentally obtained using ellipsometry measurements [9]. Fig. 1 shows our device geometry where the light of wavelength 1550 nm is guided by left silicon waveguide (height 220 nm and width 450 nm) and is coupled to plasmonic slot waveguide (slot width 140 nm) made of gold (thickness 150 nm) through a metal taper. Gold has a good property to excite SPP at visible and IR light wavelength [10]. Light of wavelength 1550 nm is guided by the left silicon waveguide and is coupled through a metal taper to the plasmonic slot waveguide filled with VO_2 in a small section. Semiconductor to metal transition in VO_2 is used to change the phase of surface plasmon polaritons (SPP) by applying a modulating voltage between the gold (Au) electrodes. The information signal has been used as a modulating voltage. A second taper is used to transforms the modulated SPP back to a photonic mode in the right silicon waveguide. This modulator has 2 working states: in the "on" mode, plasmons will propagate along the interface of VO_2 in semi-phase and gold; in the "off" mode, the plasmons will be blocked by the VO_2 in metallic phase with high absorption. Thus, this structure can realize the intensity and phase modulation. The edge coupling scheme has been utilized for coupling the light from the fiber to silicon nanowire.

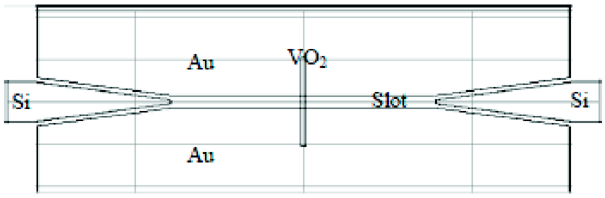

Fig. 1. Schematics of plasmonic modulator using Vanadium dioxide

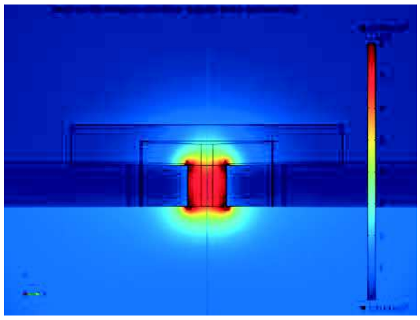
Fig. 2. Cross-sectional view of normalized E-field intensity of surface plasmon confined in the Au-VO_2-Au slot

Post-Deadline Paper ThPD2

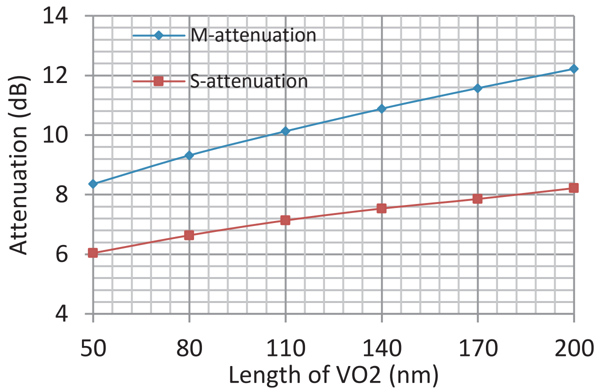

Fig. 3. Simulation results of attenuation of Metallic phase and Semi-phase with respect to length of VO2 slot

The middle section of the slot was filled with VO_2. The refractive index change accompanying the VO_2 phase change was exploited for optical phase modulation by applying an electric field between the gold electrodes in the slot waveguide. The second taper transforms the modulated surface plasmons back to photonic modes in the right silicon waveguide. Fig. 2 shows the normalized electric field of the surface plasmons confined within the gold-VO_2-gold slot at the cross-sectional cutting plane where VO_2 is in semi-phase.

Fig. 3 shows attenuation of semi-phase and metallic phase of the modulator in dB. We started sweeping the length of VO2 from 50 nm to 200 nm in order to take into account non-uniformities in the film and fabrication tolerances, with an incident light wavelength of 1550 nm. It is observed from our studies that the attenuation of 2 phases and modulation depth increased with increase in the VO_2 length.

Fig. 4 shows the variation of the modulation depth with the length of VO_2.We define the modulation depth as the metallic-phase attenuation subtracting the semi-phase attenuation. Semi-phase attenuation includes the intrinsic loss and insertion loss. The empty slot also has been simulated with incident light from 1400 nm to 1600 nm, which results have been taken as the intrinsic loss of the slot structure.

After considering the insertion loss, modulation depth, fabrication difficulty and modulation voltage, we manage to find a trade-off that the VO2 film length between 80 nm and 170 nm is desirable for the proposed modulator geometry. In current simulation, 200nm-length VO_2 slot only occupied 6.5% of whole plasmonic slot. The modulation depth can be increased by reducing the length of the plasmonic slot.

We have also swept the wavelength of incident light from 1400 nm to 1600 nm with VO_2 film length from 80nm to 170nm length. The results suggest the modulator has a broadband wavelength performance (more than 200 nm) at C-band.

The future work includes utilizing this taper coupling structure to explore the other modulation materials and the comparison of silver and gold plasmonic slot for exciting SPPs.

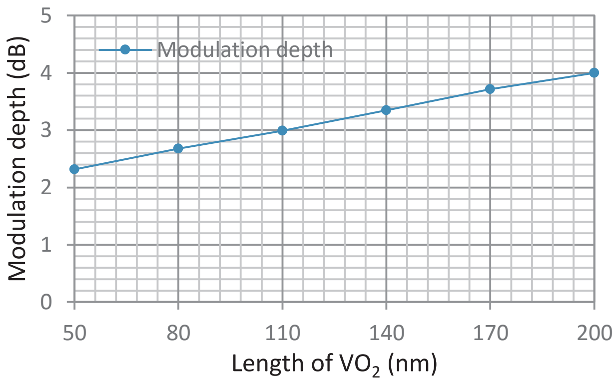

Fig. 4. Variation of modulation depth with the length of VO2 slot

III. Conclusion

We have presented a plasmonic modulator design based on VO_2, which is feasible to fabricate. The refractive index of VO_2 in the modulator is varied to route surface plasmons through either the low-loss insulating phase or high-loss metallic phase and hence to obtain low insertion loss and high modulation depth in a small footprint. Our modulator design contributes to realizing fully-integrated nanophotonic-nanoelectronic modulators in next-generation high-frequency optical communication technologies.

References

[1] MelikyanA, AlloattiL, MuslijaA, HillerkussD, P. C. Schindler, LiJ, PalmerR, KornD, MuehlbrandtS, D. Van Thourhout, ChenB, DinuR, SommerM, KoosC, KohlM, FreudeW, and LeutholdJ, "High-speed plasmonic phase modulators," Nat Photon, vol. 8, no. 3, pp. 229-233, 03//print, 2014.

[2] R. Ding, T. Baehr-Jones, Y. Liu, R. Bojko, J. Witzens, S. Huang, J. Luo, S. Benight, P. Sullivan, J. M. Fedeli, M. Fournier, L. Dalton, A. Jen, and M. Hochberg, "Demonstration of a low $V\pi L$ modulator with GHz bandwidth based on electro-optic polymer-clad silicon slot waveguides," Optics Express, vol. 18, no. 15, pp. 15618-15623, 2010/07/19, 2010.

[3] L. Alloatti, D. Korn, R. Palmer, D. Hillerkuss, J. Li, A. Barklund, R. Dinu, J. Wieland, M. Fournier, J. Fedeli, H. Yu, W. Bogaerts, P. Dumon, R. Baets, C. Koos, W. Freude, and J. Leuthold, "42.7 Gbit/s electro-optic modulator in silicon technology," Optics Express, vol. 19, no. 12, pp. 11841-11851, 2011/06/06, 2011.

[4] J.-M. Brosi, C. Koos, L. C. Andreani, M. Waldow, J. Leuthold, and W. Freude, "High-speed low-voltage electro-optic modulator with a polymer-infiltrated silicon photonic crystal waveguide," Optics Express, vol. 16, no. 6, pp. 4177-4191, 2008/03/17, 2008.

[5] P. Markov, R. E. Marvel, H. J. Conley, K. J. Miller, R. F. Haglund, and S. M. Weiss, "Optically Monitored Electrical Switching in VO2," ACS Photonics, vol. 2, no. 8, pp. 1175-1182, 2015/08/19, 2015.

[6] B. A. Kruger, A. Joushaghani, and J. K. S. Poon, "Design of electrically driven hybrid vanadium dioxide (VO2) plasmonic switches," Optics Express, vol. 20, no. 21, pp. 23598-23609, 2012/10/08, 2012.

[7] L. A. Sweatlock, and K. Diest, "Vanadium dioxide based plasmonic modulators," Optics Express, vol. 20, no. 8, pp. 8700-8709, 2012/04/09, 2012.

[8] K. J. A. Ooi, P. Bai, H. S. Chu, and L. K. Ang, "Ultracompact vanadium dioxide dual-mode plasmonic waveguide electroabsorption modulator," Nanophotonics, vol. 2, no. 1, 2013.

[9] S. K. Earl, T. D. James, T. J. Davis, J. C. McCallum, R. E. Marvel, R. F. Haglund, and A. Roberts, "Tunable optical antennas enabled by the phase transition in vanadium dioxide," Optics Express, vol. 21, no. 22, pp. 27503-27508, 2013/11/04, 2013.

[10] S. A. Maier, Plasmonics: fundamentals and applications: Springer Science & Business Media, 2007.

Exact numerical modelling for finite samples of discrete metamaterials

Mikhail Lapine
School of Mathematical and Physical Sciences
University of Technology Sydney
NSW 2007, Australia

***Abstract*—I will present the details of an exact numerical approach for precise modelling of artificial magnetic metamaterials, applicable for microwave and radio-frequency range. The pre-requisite for this modelling is a structure assembled as an array of capacitively-loaded well-conducting rings, which is most typical for microwave applications of metamaterials. The exact calculation takes all the mutual interactions into account, however a number of time-saving symmetry considerations can be applied to calculate the total impedance matrix.**

I. Introduction

Metamaterials are usually described in terms of effective material parameters [1]–[15], however it is known [16] that the real performance of practical metamaterial devices significantly deviates from theoretical predictions, even for strongly subwavelength systems. One of the reasons for that discrepancy is the finite size and finite number of individual structural elements (unit cells of metamaterial). To analyse the response of finite metamaterials with discrete structure reliably, and yet to avoid the approach of full-wave numerical simulations, a semi-analytical theory was developed, based on the circuit modelling of the structure.

I will present the details of this approach, as applied to artificial magnetic metamaterials, based on capacitively-loaded conducting rings [17]. The exact calculation takes all the mutual interactions into account, however a number of time-saving symmetry considerations can be applied to calculate the total impedance matrix.

I will then report the outcomes of such modelling with regards to the realistic metamaterial structures, and demonstrate some important differences as compared to the design predictions. More specifically, I will report new findings related to the effect of a discrete structure of practical metamaterials, as opposed to the homogenised treatment assumed in the effective medium treatment.

Indeed, one of the newly found aspects [18] is that boundary effects play a dramatic role in finite metamaterial samples with discrete structure, making their observable properties quite different from the predictions of effective medium theory. In particular, general effective medium treatments, even those tailored for a finite-thickness slabs [19], failed to describe the observable properties of metamaterial lenses limited in all the three dimensions [20].

II. Results

We now analyse the convergence of the actual properties of discrete structures towards a homogenised response, taking a spherical shape of metamaterial sample (a cubic lattice, truncated to a shape as close to a sphere as possible). For small spheres with just a few unit cells along the diameter the shape

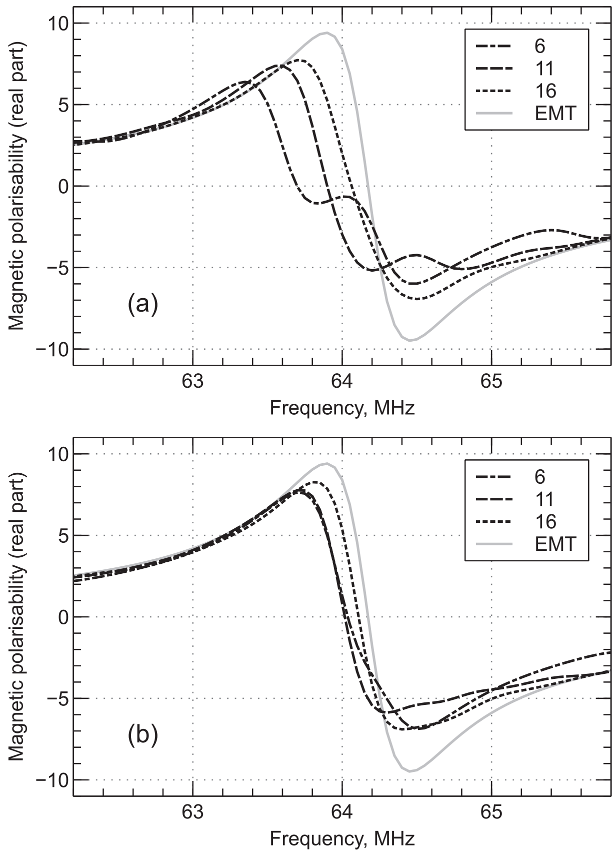

Fig. 1. Frequency dependence of the real part of the magnetic polarisability of the quasi-spherical metamaterial samples truncated from (a) “flat” or (b) “ragged” configuration of the initial boundary of the cubes. The sizes of the spheres, in terms of unit cells per diameter, is indicated by the numbers in the insets. The grey solid curve shows the polarisation theoretically calculated for a homogeneous sphere with the effective permeability [21] corresponding to the considered metamaterial structure.

Post-Deadline Paper ThPD3

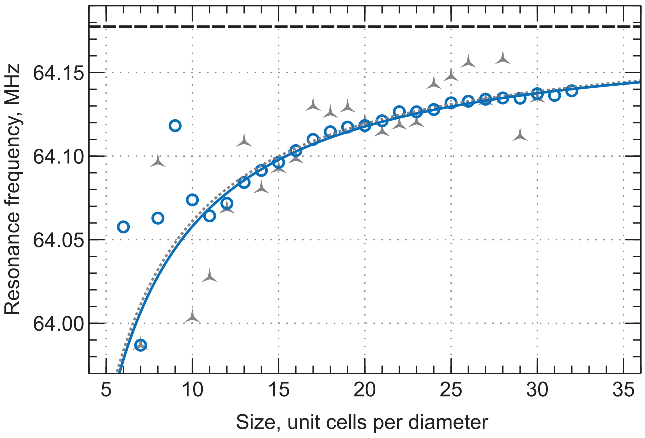

Fig. 2. Resonance frequency of the magnetic polarisability of the discrete spherical samples, depending on their size (symbols), and the corresponding convergence fits (lines), for the case of uniaxial structure with regular (blue circles, solid line) or low (grey stars, dotted line) dissipation. Theoretical frequency of the resonance is shown by black horizontal dash.

is remarkably ragged, however larger spheres appear reasonably smooth overall, with a good visual spherical appearance for sizes exceeding about 15 unit cells per diameter.

We directly calculate the response of this structure to applied field, taking all the mutual interactions between the loops into account [22]. We have observed that the calculated magnetisation curves (Fig. 1) for small discrete samples show remarkable deviations and less trivial frequency dependence, however the convergence towards the continuous model improves with size and becomes a clear trend for sizes above 11, and the results for the spheres of 16 and larger appear very similar to each other.

Although we have no computational tools to calculate much larger samples, the analysis of the convergence trend towards the effective medium theory (Fig. 2) allows us to conclude that eventually the difference between a discrete sphere and a continuous one can be eliminated to good precision.

III. Conclusion

The effects outlined above are particularly prominent in metamaterials with strongly interacting elements, such as those based on ring resonators. It also appears that having a resonance is essential for boundary effects to spread through the structure. Indeed, as opposed to resonant metamaterials, response of artificial diamagnetics of finite size and discrete structure is in a good agreement with the effective medium predictions. Our conclusions are likely to be rather general, applicable in a wide frequency range and for many specific designs, so these results may have severe implications for practical development of metamaterials.

Acknowledgment

This work was supported by Australian Research Council (CUDOS, CE110001018).

References

[1] V. M. Agranovich and Y. N. Gartstein, “Electrodynamics of metamaterials and the Landau-Lifshitz approach to the magnetic permeability,” *Metamaterials*, vol. 3, pp. 1–9, 2009.

[2] C. R. Simovski, “Material parameters of metamaterials (a review),” *Optics and Spectroscopy*, vol. 107, no. 5, pp. 726–753, 2009.

[3] A. Vinogradov, D. Makhnovskii, and K. Rozanov, “Effective boundary layer in composite materials,” *J. Commun. Technol. Electron.*, vol. 44, no. 3, pp. 317–322, 1999.

[4] A. Sarychev, R. McPhedran, and V. Shalev, “Electrodynamics of metal-dielectric composites and electromagnetic crystals,” *Phys. Rev. B*, vol. 62, no. 12, pp. 8531–8539, 2000.

[5] M. Gorkunov, M. Lapine, E. Shamonina, and K. H. Ringhofer, “Effective magnetic properties of a composite material with circular conductive elements,” *Eur. Phys. J. B*, vol. 28, pp. 263–269, 2002.

[6] P. A. Belov, R. Marqués, S. I. Maslovski, I. S. Nefedov, M. Silveirinha, C. R. Simovski, and S. A. Tretyakov, “Strong spatial dispersion in wire media in the very large wavelength limit,” *Phys. Rev. B*, vol. 67, p. 113103, 2003.

[7] M. A. Shapiro, G. Shvets, J. R. Sirigiri, and R. J. Temkin, “Spatial dispersion in metamaterials with negative dielectric permittivity and its effect on surface waves,” *Opt. Lett.*, vol. 31, no. 13, pp. 2051–2053, 2006.

[8] M. Silveirinha, “Metamaterial homogenization approach with application to the characterization of microstructured composites with negative parameters,” *Phys. Rev. B*, vol. 75, p. 115104, 2007.

[9] P. Ikonen, E. Saenz, R. Gonzalo, C. Simovski, and S. Tretyakov, “Mesoscopic effective material parameters for thin layers modeled as single and double grids of interacting loaded wires,” *Metamaterials*, vol. 1, no. 2, pp. 89–105, 2007.

[10] M. Silveirinha, J. Baena, L. Jelinek, and R. Marques, “Nonlocal homogenization of an array of cubic particles made of resonant rings,” *Metamaterials*, vol. 3, pp. 115–128, 2009.

[11] W. Perrins and R. McPhedran, “Metamaterials and the homogenization of composite materials,” *Metamaterials*, vol. 4, pp. 24–31, 2010.

[12] A. Alù, “First-principles homogenization theory for periodic metamaterials,” *Phys. Rev. B*, vol. 84, p. 075153, 2011.

[13] A. S. Andryieuski, S. Ha, A. A. Sukhorukov, Y. S. Kivshar, and A. V. Lavrinenko, “Bloch-mode analysis for retrieving effective parameters of metamaterials,” *Phys. Rev. B*, vol. 86, p. 035127, 2012.

[14] A. Chipouline, C. Simovski, and S. Tretyakov, “Basics of averaging of the maxwell equations for bulk materials,” *Metamaterials*, vol. 6, no. 3-4, pp. 77–120, 2012.

[15] J. Vehmas, S. Hrabar, and S. Tretyakov, “Omega transmission lines with applications to effective medium models of metamaterials,” *J. Appl. Phys.*, vol. 115, p. 134905, 2014.

[16] C. R. Simovski, “On electromagnetic characterization and homogenization of nanostructured metamaterials,” *Journal of Optics*, vol. 13, no. 1, p. 013001, 2011.

[17] R. Marqués, L. Jelinek, M. Freire, J. Baena, and M. Lapine, “Bulk metamaterials made of resonant rings,” *Proc. IEEE*, vol. 99, pp. 1660–1668, 2011.

[18] M. Lapine, L. Jelinek, and R. Marqués, “Surface mesoscopic effects in finite metamaterials,” *Opt. Express*, vol. 20, no. 16, pp. 18 297–18 302, 2012.

[19] L. Jelinek, R. Marques, and M. Freire, “Accurate modeling of split ring metamaterial lenses for magnetic resonance imaging applications,” *J. Appl. Phys.*, vol. 105, p. 024907, 2009.

[20] M. Lapine, L. Jelinek, M. Freire, and R. Marqués, “Realistic metamaterial lenses: Limitations imposed by discrete structure,” *Phys. Rev. B*, vol. 82, p. 165124, 2010.

[21] J. D. Baena, L. Jelinek, R. Marqués, and M. Silveirinha, “Unified homogenization theory for magnetoinductive and electromagnetic waves in split-ring metamaterials,” *Phys. Rev. A*, vol. 78, p. 013842, 2008.

[22] M. Lapine, L. Jelinek, R. Marqués, and M. Freire, “Exact modelling method for discrete finite metamaterial lens,” *IET Microw. Antenn. Propag.*, vol. 4, pp. 1132–1139, 2010.